ACADEMIA ROMÂNĂ
*Revue Roumaine de Chimie*
http://web.icf.ro/rrch/

*Rev. Roum. Chim.*,
**2015**, *60*(10), 1005-1013

# INTERPLAY OF HYDROGEN BOND AND STACKING INTERACTIONS IN THE CRYSTAL STRUCTURE OF A NEW MONONUCLEAR ZINC COMPLEX

Andrei CUCOS,[a] Carmen PARASCHIV,[a,*] Sergiu SHOVA,[b] Augustin MADALAN,[c] Gabriela SBARCEA,[a] Virgil MARINESCU[a] and Marius ANDRUH[c,*]

[a] National Institute for Research and Development in Electrical Engineering ICPE-CA, 313 Splaiul Unirii, 030138-Bucharest, Roumania
[b] "Petru Poni" Institute of Macromolecular Chemistry of the Roumanian Academy, 41-A Grigore Ghica Voda Alley, RO-700487 Iaşi, Roumania
[c] Inorganic Chemistry Laboratory, Faculty of Chemistry, University of Bucharest, 23 Dumbrava Roşie Str., 020464-Bucharest, Roumania

*Received August 6, 2015*

A new mononuclear complex, $[Zn(H_3tris)_2(bpe)]_2\cdot(bpe)_2\cdot(NO_3)_4$ **1** ($H_3tris$ = tris(hydroxymethyl)aminomethane, bpe = 1,2-bis(4-pyridyl)ethylene), has been synthesized solvothermally. Its crystal structure, thermogravimetric analysis, solid-state transformation to ZnO and characterization of the resulted zinc oxide material are reported. The structure consists of $[Zn(H_3tris)_2(bpe)]^{2+}$ mononuclear dicationic species, uncoordinated bpe molecules and nitrate anions. The crystallographic investigation reveals the formation of one-dimensional chains based upon N-H···N hydrogen bond interactions between the amino nitrogens coordinated to the zinc atoms and the bpe ligand from an adjacent mononuclear entity. The π-π stacking interactions established between the aromatic fragments of the coordinated and uncoordinated bpe molecules also play an important role in sustaining the supramolecular solid-state architecture. Furthermore, a 3-D supramolecular network is formed through plentiful hydrogen bonds involving the ligands, the guest molecules and the nitrate counteranions.

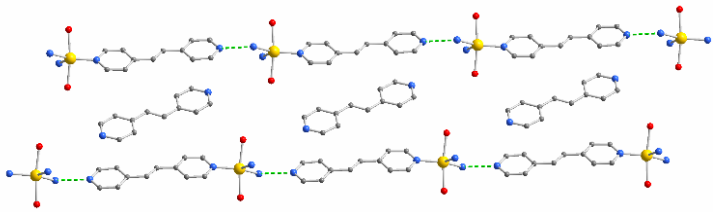

## INTRODUCTION

Metal directed formation of molecules is governed by the coordination geometry of the metal ion and influenced by various non-covalent forces, mainly originating from the structural features of the ligands. Hydrogen bonds and π–π stacking interactions are important supramolecular tools that can contribute to a fast and reversible assembly of molecules and have been encountered in numerous systems reported so far.[1,2]

Rigid rod-like molecules have been widely employed as tectons in supramolecular chemistry and crystal engineering. Among them, aromatic nitrogen containing ligands such as 4,4'-bipyridine[3] and bis(4-pyridyl) derivatives *(e.g.* 1,2-bi(4-pyridyl)ethane,[4] 1,2-bis(4-pyridyl)ethylene,[5] bis(4-pyridyl)acetylene,[6] 1,4-bis(4-pyridyl)benzene[7]) have been used for the construction of numerous coordination polymers with various dimensionalities and network topologies. These molecules can act as ligands (bridging or monodentate) or can be found as guests in the crystal lattice. At the supramolecular level, they are able to act as hydrogen bond acceptors through the pyridyl nitrogen atoms and also to be involved in π–π stacking interactions through the aromatic moieties.[8]

* Corresponding authors: carmenparaschiv@yahoo.com (C.P.); marius.andruh@dnt.ro (M.A.)

In a series of papers, we have shown that alkoxo-bridged Cu(II) cationic species can be used as nodes in constructing extended structures by connecting them through a large variety of aromatic nitrogen containing spacers.[9] As a continuation to this research, we decided to employ the Zn(II) ion for the construction of coordination polymers based on amino-alcohols and different bis(4-pyridyl) derivatives. In the present paper we focus on the interplay of hydrogen bonding and aromatic-aromatic interactions in the crystal structure of a mononuclear complex, $[Zn(H_3tris)_2(bpe)]_2 \cdot (bpe)_2 \cdot (NO_3)_4$ **1**.

## RESULTS AND DISCUSSION

Compound **1** crystallizes in the *P*-1 triclinic space group, with cell parameters and structure refinement details given in Table 1. The asymmetric unit consists of two chemically identical but crystallographically non-equivalent $[Zn(H_3tris)_2(bpe)]^{2+}$ cations, two uncoordinated bpe molecules and four nitrate anions (Fig. 1). Both metal ions Zn1 and Zn2, as well as one of the OH groups of each $H_3$tris ligand, are disordered between two resolvable positions having the same relative occupancies of 0.9:0.1 ratios. Hence, only the major component of the structure will be discussed below. The $H_3$tris molecules are not deprotonated and coordinate as bidentate chelating ligands toward the zinc ions, involving the nitrogen and one oxygen atom, while the other two OH groups remain uncoordinated. The slight differences between the two mononuclear complex dications concern the stereochemistry of the zinc atoms. Both are five-coordinated by two oxygen and two nitrogen atoms from the $H_3$tris bidentate ligands and an oxygen atom from a monodentate bpe molecule, showing distorted square pyramidal geometry, with the trigonal distortion parameters $\tau$[10] equal to 0.45 (for Zn1) and 0.39 (for Zn2). The Zn–O distances vary from 2.170(2) to 2.187(2) Å, while the Zn–N bonds are in the 2.009(3) – 2.079(3) range. Selected bond distances and angles for compound **1** are presented in Table 2.

The mononuclear entities are interconnected through N-H···N hydrogen bonds established between the amino nitrogen atom from the $H_3$tris ligand and the uncoordinated pyridyl nitrogen atom from an adjacent mononuclear complex [N1···N4′ = 3.026 Å; N8···N5′ = 2.983 Å; ′ = x, 1+y, z] to afford supramolecular chains running along the crystallographic *b* axis (Fig. 2).

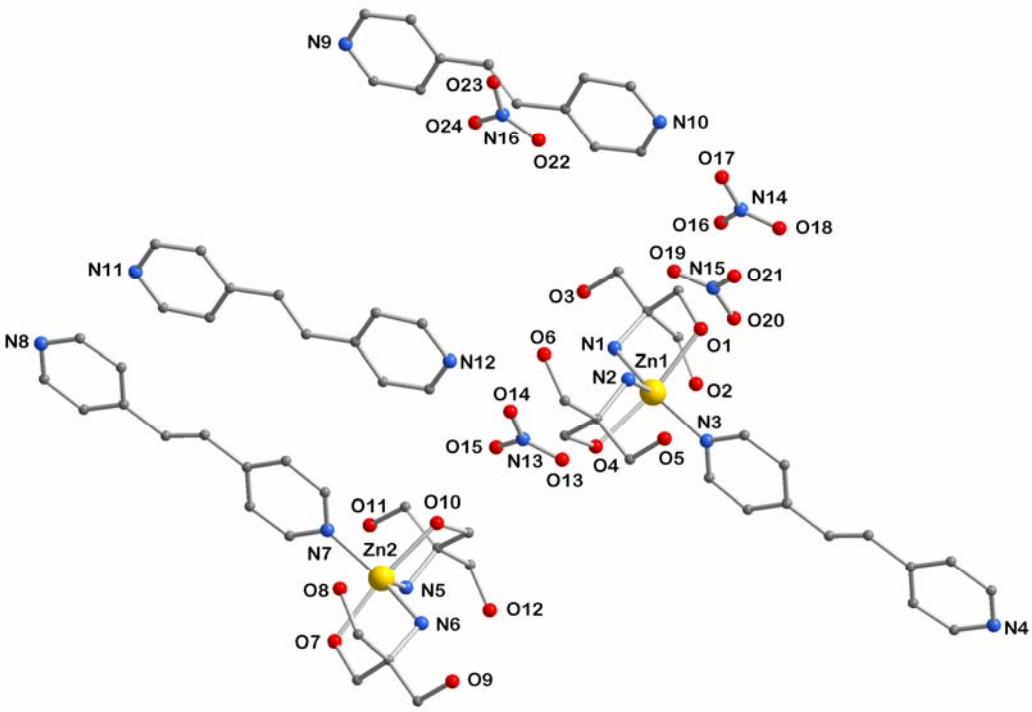


Fig. 1 – The asymmetric unit in **1** with the atom labeling scheme. Only the major occupational sites (refined at 0.9 for Zn1 and Zn2) are shown. Hydrogen atoms have been omitted.

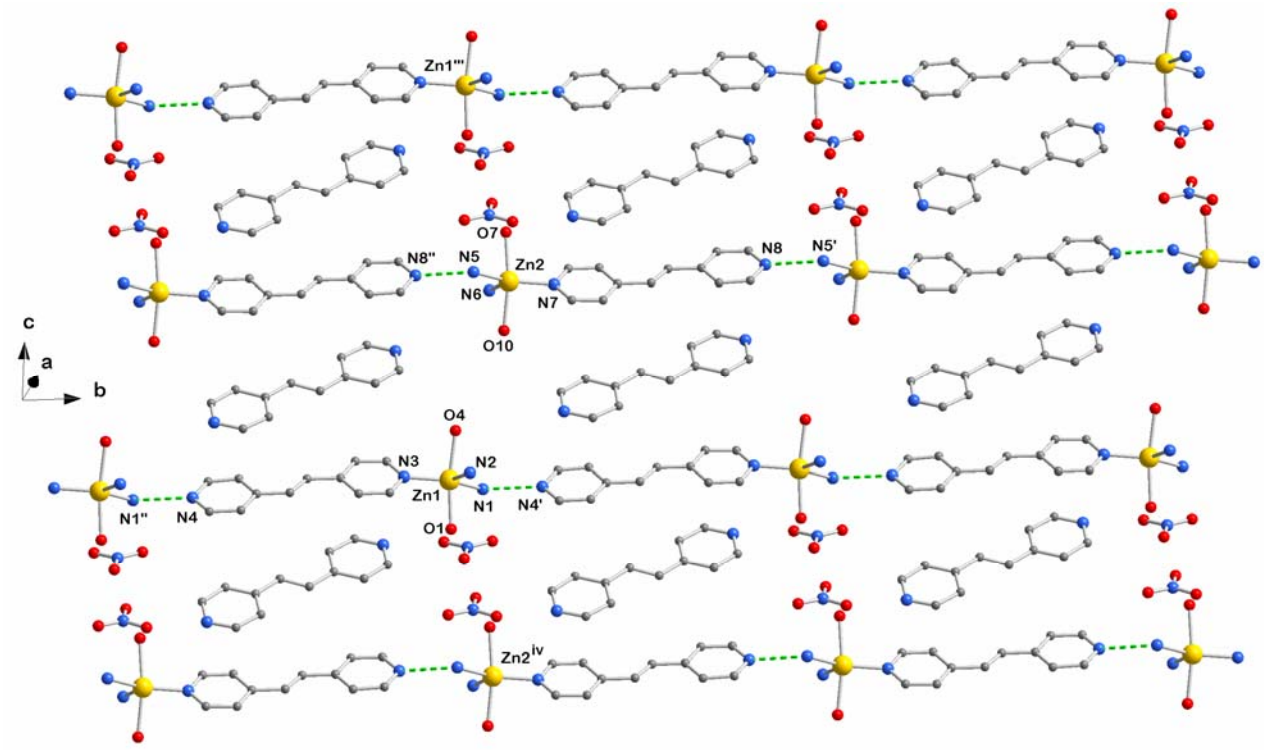


Fig. 2 – Supramolecular 1-D chains running along the crystallographic *b* axis (symmetry transformations: ′ = x, 1+y, z; ″ = x, -1+y, z; ‴ = x, y, 1+z; iv = x, y, -1+z). The C atoms and uncoordinated OH groups from the $H_3$tris ligands have been omitted for clarity.

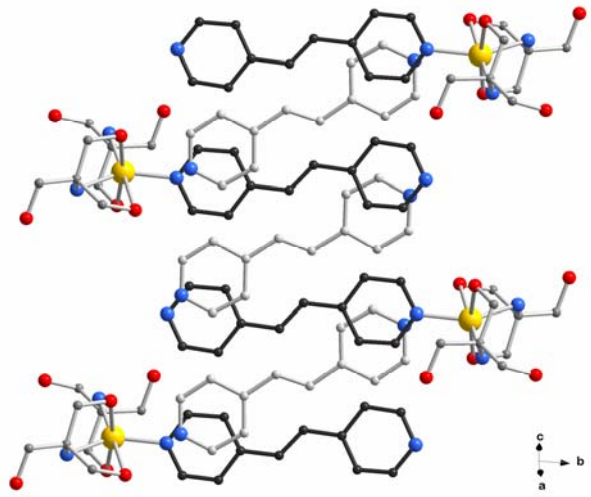


Fig. 3 – Detail of the packing diagram showing the head-to-tail π-π interactions between the coordinated (dark grey) and guest (light grey) bpe molecules.

The analysis of the packing diagram reveals the presence of π-π interactions between the coordinated and the guest bpe molecules. Each coordinated bpe ligand interacts with two uncoordinated bpe molecules lying above and below in a head-to-tail fashion, resulting in infinite columns along the crystallographic *c* axis (Fig. 3). The aromatic moieties are stacked in an almost parallel displaced mode, with dihedral angles between 4.3 and 6.4º and distances between the rings from 3.33 to 3.79 Å, being in the range observed with other systems described in the literature.

The structure is stabilized by an extensive 3-D network of hydrogen bonds, which involve the OH groups (both coordinated and uncoordinated) and the amino nitrogen atoms from the $H_3$tris ligands, the pyridyl nitrogens and the nitrate anions (Fig. 4). The O···O distances range from 2.59 to 2.81 Å, while the O···N separations vary between 2.80 and 3.03 Å. Details of the H-bonding parameters for **1** are given in Table 3.

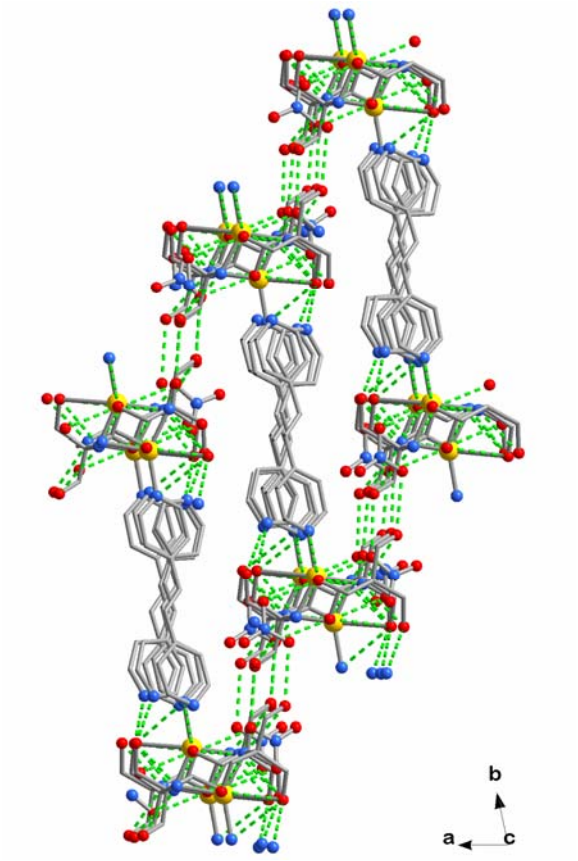


Fig. 4 – Fragment of the packing diagram showing the 3-D hydrogen bonded network.

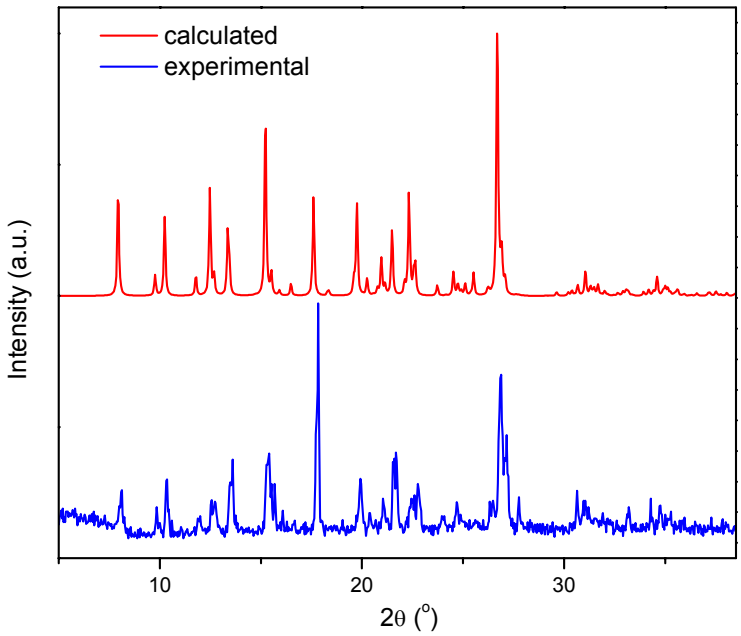


Fig. 5 – Powder X-ray diffraction patterns of **1**. Above: calculated from single crystal diffraction data; below: experimental data.

Powder X-ray diffraction has been used to verify the phase purity of the synthesized sample in solid state. The simulated and experimental powder X-ray diffraction patterns of complex **1** are in good agreement with each other, indicating the phase purity of the product as shown in Fig. 5.

## Thermal stability studies

The TG analysis (Fig. 6) has shown that compound **1** is thermally stable up to around 210 ºC. On further heating the decomposition starts, being characterized by two main processes. The first

has a sharp minimum in DTG at 260 ºC, being accompanied by an exothermic shoulder in the DTA curve and a peak in the Gram Schmidt curve at 266 ºC. The second mass loss, which occurs at above 500 ºC (DTG peak at 531 ºC), is due to the combustion of the organic residues, leading to a strong exothermic peak at 532 ºC and an intense maximum in the Gram Schmidt curve at 535 ºC. The decomposition is complete at 570 ºC, yielding the expected amount of ZnO residue (calculated: 10.2%, found: 10.5%).

The 2D plot of the FTIR spectra of evolved gases is presented in Fig. 7. In the first decomposition process several volatiles are released, as evidenced by the observation of the characteristic and strong bands of $CO_2$ (2200 – 2400 $cm^{-1}$, 600 – 750 and 3500 – 3750 $cm^{-1}$ regions), $H_2O$ vapors (series of narrow bands at 4000-3500, 2000-1300 $cm^{-1}$) and $NH_3$ (characteristic bands at 964 and 930 $cm^{-1}$, series of narrow bands at 1200 – 750 $cm^{-1}$) that are formed mainly from the decomposition of $H_3$tris ligands, and of small amounts of $N_2O$, that may originate from the nitrate anions. Between 350–400 ºC the weak bands of pyridine (3080, 1580, 1440 $cm^{-1}$) are visible, suggesting the decomposition of bpe molecules. Finally, at about 500 ºC, a new and more intense release of $CO_2$ and $N_2O$ is observed, together with slight amounts of $H_2O$ and NO (1909, 1850 $cm^{-1}$), corresponding to the second mass loss due to the combustion of the organic residues.

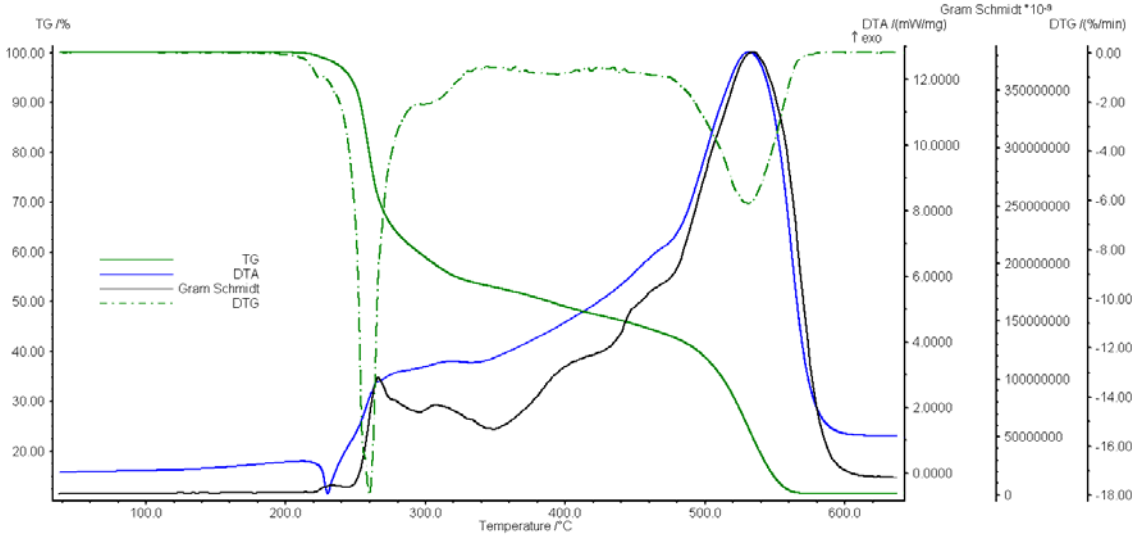


Fig. 6 – TG, DTG, DTA and Gram Schmidt curves for compound **1**.

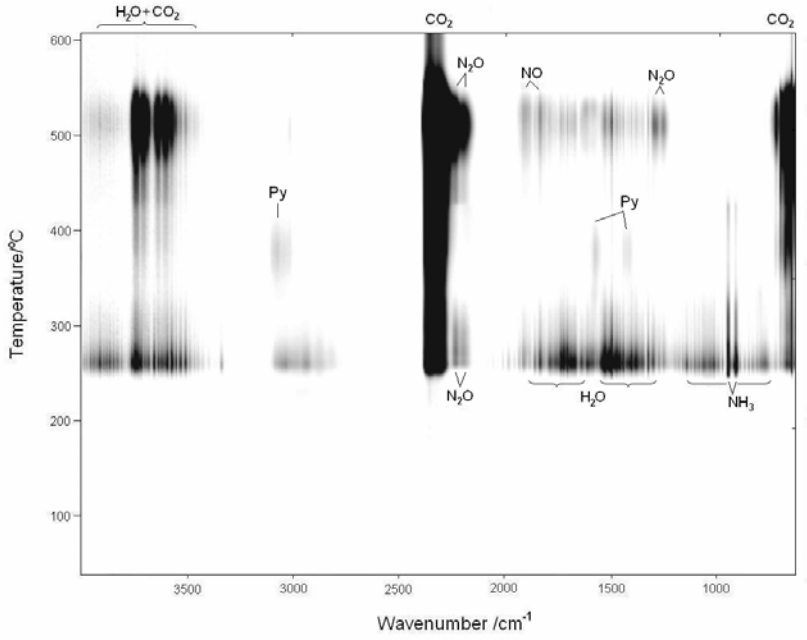


Fig. 7 – 2D plot of FTIR spectra of evolved gases from the decomposition of **1**.

### Conversion to ZnO

The zinc oxide generated upon calcination in air of compound **1** at 600 °C for 1 h was studied by PXRD and scanning electron microscopy (SEM).

The XRD pattern match with the typical hexagonal phase of the wurtzite structure of ZnO. The sharp diffraction peaks indicate a good crystallinity of the ZnO particles. No other peaks related to any impurity were observed.

Investigation of the SEM images revealed aggregates of particles having asymmetric hexagonal shapes, with rounded edges and diameters from 130 to 550 nm.

In this work a supramolecular Zn(II) system based on amino-alcohol tris(hydroxymethyl)aminomethane and the N-donor spacer 1,2-bis(4-pyridyl)ethylene was studied. The interplay of non-covalent interactions such as π–π stacking and hydrogen bonding influence the structural organization and crystal packing.

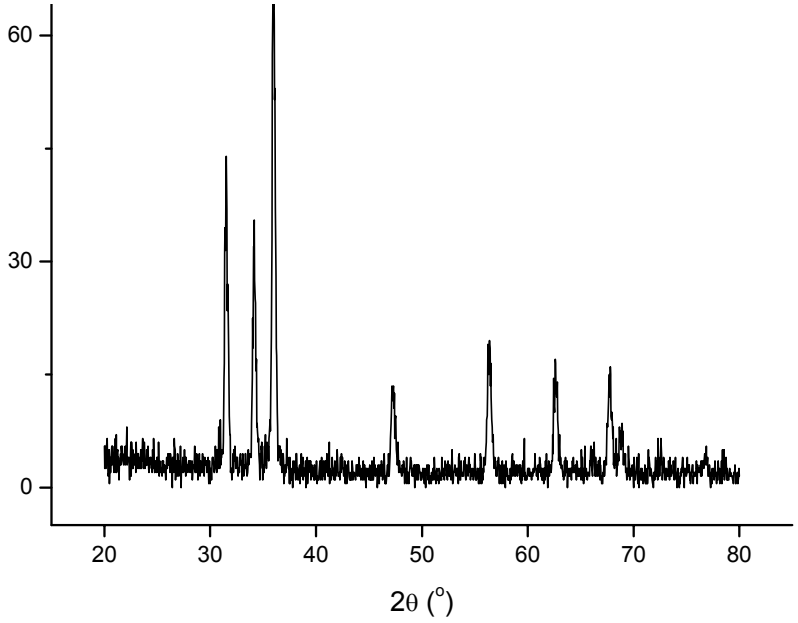


Fig. 8 – Powder X-ray diffraction pattern of the ZnO generated upon calcination of **1**.

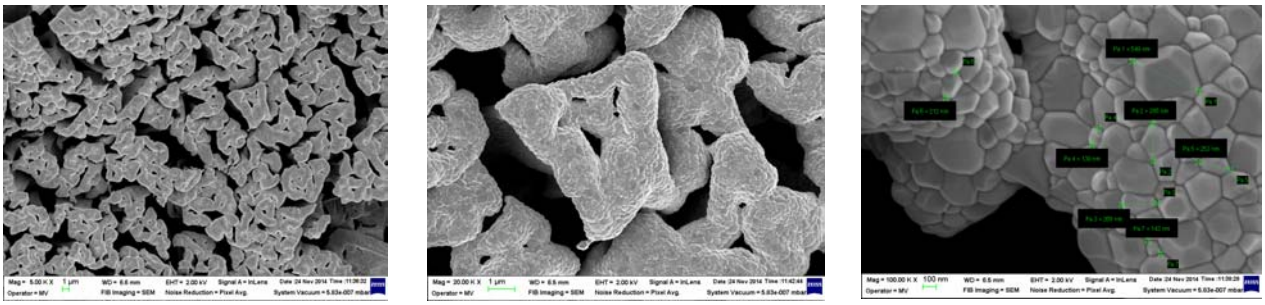

Fig. 9 – SEM images at different magnifications for ZnO particles.

*Table 1*

Crystallographic data and structure refinement parameters for **1**

| | **1a** |
|---|---|
| Empirical formula | $C_{32}H_{42}ZnN_8O_{12}$ |
| *M* | 796.11 |
| Temperature [K] | 160.0(1) |
| Wavelength [Å] | 0.71073 |
| Crystal system | triclinic |
| Space group | *P -1* |
| *a* [Å] | 14.7328(8) |

*Table 1 (continued)*

| | |
|---|---|
| $b$ [Å] | 15.4033(7) |
| $c$ [Å] | 17.4394(9) |
| $\alpha$ [°] | 85.783(4) |
| $\beta$ [°] | 65.108(5) |
| $\gamma$ [°] | 77.342(4) |
| $V$ [Å$^3$] | 3501.9(3) |
| $Z$ | 2 |
| $\rho$(calcd) [Mgm$^{-3}$] | 1.510 |
| $\mu$ [mm$^{-1}$] | 0.777 |
| Crystal size/mm$^3$ | 0.70 × 0.40 × 0.40 |
| $\theta_{min,}$ $\theta_{max}$(°) | 3.1 to 50.06 |
| Reflections collected | 24447 |
| Independent reflections | 12352 [$R_{int}$ = 0.0419] |
| Data/restraints/parameters | 12352/28/979 |
| $R_1{}^a(I > 2\sigma(I)$ | 0.0485 |
| $wR_2{}^b$(all data) | 0.1301 |
| Gof | 0.995 |
| Largest diff. peak/hole/e Å$^{-3}$ | 0.46/-0.56 |

*Table 2*

Selected bond distances (Å) and angles (º) for compound **1**

| | | | |
|---|---|---|---|
| Zn1–O1 | 2.170(2) | O1–Zn1–O4 | 170.70(10) |
| Zn1–O4 | 2.187(2) | N1–Zn1–O1 | 80.55(10) |
| Zn1–N1 | 2.013(3) | N1–Zn1–O4 | 94.82(10) |
| Zn1–N2 | 2.064(3) | N1–Zn1–N2 | 107.03(12) |
| Zn1–N3 | 2.010(3) | N2–Zn1–O1 | 93.84(10) |
| Zn1X–N1 | 1.914(5) | N2–Zn1–O4 | 79.73(10) |
| Zn1X–N2 | 1.948(5) | N3–Zn1–O1 | 95.48(10) |
| Zn1X–N4$^{i}$ | 1.914(5) | N3–Zn1–O4 | 92.99(11) |
| Zn2–O7 | 2.179(2) | N3–Zn1–N1 | 143.87(12) |
| Zn2–O10 | 2.175(2) | N3–Zn1–N2 | 109.08(12) |
| Zn2–N5 | 2.024(3) | N1–Zn1X–N2 | 116.2(3) |
| Zn2–N6 | 2.079(3) | N1–Zn1X–N4$^{i}$ | 104.4(2) |
| Zn2–N7 | 2.009(3) | N2–Zn1X–N4$^{i}$ | 138.7(3) |
| Zn2X–N5 | 1.966(6) | N5–Zn2–O7 | 80.42(10) |
| Zn2X–N6 | 1.950(6) | N5–Zn2–O10 | 95.14(10) |
| Zn2X–N8$^{ii}$ | 1.889(6) | N5–Zn2–N6 | 105.85(12) |
| | | N6–Zn2–O7 | 93.54(10) |
| | | N6–Zn2–O10 | 79.47(10) |
| | | N7–Zn2–O7 | 96.35(11) |
| | | N7–Zn2–O10 | 91.97(11) |
| | | N7–Zn2–N5 | 146.80(12) |
| | | N7–Zn2–N6 | 107.33(12) |
| | | N6–Zn2X–N5 | 113.4(3) |
| | | N5–Zn2X–N8$^{ii}$ | 101.3(3) |
| | | N6–Zn2X–N8$^{ii}$ | 143.6(3) |

$^{i}$ = x, 1+y, z
$^{ii}$ = x, -1+y, z

## EXPERIMENTAL

### Materials and methods

All starting materials were of reagent grade quality and were used as received from commercial sources without further purification.

A mixture of $Zn(NO_3)_2{\cdot}6H_2O$ (0.3 g, 1 mmol), $H_3$tris (0.24 g, 2 mmol), and bis(4-pyridyl)ethylene (0.18 g, 1 mmol) in methanol (20 mL) was sealed in a Teflon-lined stainless steel container and heated at 110 ºC for 30 hours, then slowly cooled to room temperature. The resulted yellow crystals were washed with methanol and dried in air. Yield: 68%. Elemental chemical analysis: 48.28% C, 5.32% H, 14.08%, N (calcd); 48.17% C, 5.71% H, 14.43%, N (found). IR (cm$^{-1}$, KBr): 3373w, 3305w, 3042m, 2934w, 2826w, 1618m, 1602s, 1437m, 1384vs, 1342m, 1070m, 1029m, 1001m, 827m, 552m.

### Physical measurements

The IR spectrum was recorded on KBr pellets in the 4000-400 cm$^{-1}$ range using a Bruker TENSOR 27 FTIR Spectrometer. Elemental analyses (C, H, N) were performed on EuroVector EA3000 CHNS-O Elemental Analyzer. PXRD

diffractions pattern was recorded on a Bruker D8 ADVANCE diffractometer. The TG/DTG/DTA+FTIR measurement was performed on a Netzsch STA 409 PC thermal analyzer coupled to a Bruker Tensor 27 FTIR spectrometer equipped with a TG-IR gas cell. The sample was placed in a cylindrical $Al_2O_3$ holder and heated in synthetic air flow (100 ml $min^{-1}$, purity 99.999%), from room temperature to 600 °C, at a heating rate of 10 °C $min^{-1}$. An empty $Al_2O_3$ holder was used as reference. The FTIR spectra were collected continuously during measurements in the wavenumber range 4000 – 650 $cm^{-1}$ at a resolution of 4 $cm^{-1}$. The SEM measurements were carried out on a Carl Zeiss SMT FESEM-FIB Workstation Auriga.

**Crystal structure determination**

Crystallographic measurements for **1** were carried out with an Oxford-Diffraction XCALIBUR E CCD diffractometer equipped with graphite-monochromated Mo Ka radiation. Single crystals were positioned at 40 mm from the detector and 401 frames were measured each for 6 s over 1° scan width. The unit cell determination and data integration were carried out using the CrysAlis package of Oxford Diffraction.[11] All the structures were solved by direct methods using Olex2[12] software with the SHELXS structure solution program and refined by full-matrix least-squares on F2 with SHELXL-97.[13] The solution of the crystal structure resulted clearly into the $[Zn(H_3tris)_2(bpe)]^{2+}$ mononuclear dicationic species. However, the subsequent calculations of $\Delta F$ maps has revealed the presence of quite strong residual electron density at the level of $\Delta\rho max \sim 6$ e/Å3, located at the center of polyhedron described by N1, N2, disordered O1x, O4x and symmetrical N4($x$, 1 + $y$, $z$) atoms for Zn1x metal position and N5, N6, disordered O7x, O10x and symmetrical N8($x$, -1 + $y$, $z$) atoms for Zn2x position. At this point, it was assumed that two peaks correspond to the second positions of Zn1 and Zn2 atoms with the suitable values for the Zn-O and Zn-N distances. The further refinement of the structure has shown that the value of *s.o.f.* for both Zn1x and Zn2x positions is very low, being equal to 0.1. Atomic displacements for non-hydrogen atoms were refined using an anisotropic model. Hydrogen atoms were placed in fixed, idealized positions and refined as rigidly bonded to their corresponding atoms. Hydrogen atoms for OH and $NH_2$ groups have been placed by Fourier Difference, accounting for the hybridization and the hydrogen bonds parameters. CCDC-1419953 contains the supplementary crystallographic data. These data can be obtained free of charge from The Cambridge Crystallographic Data Centre via www.ccdc.cam.ac.uk/data_request/cif.

*Acknowledgements*: Financial support from the Roumanian Ministry of Education CNCS-UEFISCDI (Project PN-II-RUTE-2012-3-0390) is gratefully acknowledged.

## REFERENCES

1. (a) G. R. Desiraju, *Angew. Chem. Int. Ed.*, **1995**, *34*, 2311; (b) G. R. Desiraju, *Acc. Chem. Res.*, **2002**, *35*, 565; (c) G. R. Desiraju, in: F. Vögtle, J. F. Stoddart and M. Shibasaki (Eds.), "Stimulating Concepts in Chemistry", Wiley VCH, Weinheim, 2000, p. 293; (d) M. C. Etter, *Acc. Chem. Res*., **1990**, *23*, 120; (e) M. C. Etter, *J. Phys. Chem*., **1991**, *95*, 4601; (f) A. M. Beatty, *Coord. Chem. Rev*., **2003**, *246*, 131; (g) C. B. Aakeröy and K. R. Seddon, *Chem. Soc. Rev*., **1993**, *22*, 397; (h) L. Brammer, *Chem. Soc. Rev*., **2004**, *43*, 476; (i) D. Braga, F. Grepioni and G. R. Desiraju, *Chem. Rev*., **1998**, *98*, 1375; (j) M. J. Zaworotko, *Chem. Soc. Rev*., **1994**, *23*, 283; (k) S. Kitagawa and K. Uemura, *Chem. Soc. Rev*., **2005**, *34*, 109; (l) B. Moulton and M. J. Zaworotko, *Chem. Rev*., **2001**, *101*, 1629; (m) T. Steiner, *Angew. Chem. Int. Ed.*, **2002**, *41*, 48.
2. (a) C. Janiak, *J. Chem. Soc., Dalton Trans.*, **2000**, 3885; (b) T. Caronna, R. Liantonio, T. A. Logothetis, P. Metrangolo, T. Pilati and G. Resnati, *J. Am. Chem. Soc.*, **2004**, *126*, 4500; (c) S. Grimme, *Angew. Chem. Int. Ed.*, **2008**, *47*, 3430; (d) S. L. Crockroft, C. A. Hunter, K. R. Lawson, J. Perkins and C. J. Urch, *J. Am. Chem. Soc.*, **2005**, *127*, 8594.
3. (a) M. J. Zaworotko, *Cryst. Growth Des*., **2007**, *7*, 4; (b) K. Biradha, M. Sarkar and L. Rajput, *Chem. Commun.*, **2006**, 4169; (c) M. Fujita, Y. J. Kwon, S. Washizu and K. Ogura, *J. Am. Chem. Soc.*, **1994**, *116*, 1151; (d) N. N. Adarsh and P. Dastidar, *Chem. Soc. Rev*., **2012**, *41*, 3039.
4. (a) P. S. Mukherjee, S. Konar, E. Zangrando, T. Mallah, J. Ribas and N. R. Chaudhuri, *Inorg. Chem.*, **2003**, *42*, 2695; (b) R. Carballo, B. Covelo, M. S. El Fallah, J. Ribas and E. M. Vázquez-López, *Cryst. Growth Des.*, **2007**, *7*, 1069; (c) X.-H. Chang, J.-H. Qin, L.-F. Ma, J.-G. Wang and L.-Y. Wang, *Cryst. Growth Des.*, **2012**, *12*, 4649; (d) I. H. Hwang, H.-Y. Kim, M. M. Lee, Y. J. Na, J. H. Kim, H.-C. Kim, C. Kim, S. Huh, Y. Kim and S.-J. Kim, *Cryst. Growth Des.*, **2013**, *13*, 4815; (e) N. de la Pinta, S. Martín, M. K. Urtiaga, M. G. Barandika, M. I. Arriortua, L. Lezama, G. Madariaga and R. Cortés, *Inorg. Chem.*, **2010**, *49*, 10445; (f) D. Ghoshal, T. K. Maji, G. Mostafa, T.-H. Lu and N. R. Chaudhuri, *Cryst. Growth Des.*, **2003**, *3*, 9.
5. (a) G. Li, H. Hou, L. Li, X. Meng, Y. Fan and Y. Zhu, *Inorg. Chem.*, **2003**, *42*, 4995; (b) U. García-Couceiro, O. Castillo, J. Cepeda, M. Lanchas, A. Luque, S. Pérez-Yáñez, P. Román and D. Vallejo-Sánchez, *Inorg. Chem.*, **2010**, *49*, 11346; (c) W. Wong-Ng, J. T. Culp, Y. S. Chen, P. Zavalij, L. Espinal, D. W. Siderius, A. J. Allen, S. Scheins and C. Matranga, *Cryst. Eng. Comm.*, **2013**, *15*, 4684; (d) C. M. Nagaraja, B. Ugale and A. Chanthapally, *Cryst. Eng. Comm.*, **2014**, *16*, 4805.
6. (a) A. Akou, C. Bartual-Murgui, K. Abdul-Kader, M. Lopes, G. Molnár, C. Thibault, C. Vieu, L. Salmon and A. Bousseksou, *Dalton Trans.*, **2013**, *42*, 16021; (b) S. Welsch, C. Lescop, M. Scheer and R. Réau, *Inorg. Chem.*, **2008**, *47*, 8592; (c) Y.-B. Dong, R. C. Layland, N. G. Pschirer, M. D. Smith, U. H. F. Bunz and H.-C. zur Loye, *Chem. Mater.*, **1999**, *11*, 1413; (d) Y.-B. Dong, R. C. Layland, M. D. Smith, N. G. Pschirer, U. H. F. Bunz and H.-C. zur Loye, *Inorg. Chem.*, **1999**, *38*, 3056.
7. (a) X.-R. Wu, X. Yang, R.-J. Wei, J. Li, L.-S. Zheng and J. Tao, *Cryst. Growth Des.*, **2014**, *14*, 4891; (b) J.-Y. Li, Z. Yan, Z.-P. Ni, Z.-M. Zhang, Y.-C. Chen, W. Liu and M.-L. Tong, *Inorg. Chem.*, **2014**, *53*, 4039; (c) J. T. Culp, C. Madden, K. Kauffman, F. Shi and C. Matranga, *Inorg. Chem.*, **2013**, *52*, 4205.
8. H. W. Roesky and M. Andruh, *Coord. Chem. Rev*., **2003**, *236*, 91.
9. (a) G. Marin, M. Andruh, A. M. Madalan, A. J. Blake, C. Wilson, N. R. Champness and M. Schröder, *Cryst.*

*Growth Des.*, **2008**, *8*, 964; (b) G. Marin, V. C. Kravtsov, I. A. Simonov, V. Tudor, J. Lipkowski and M. Andruh, *J. Mol. Struct.*, **2006**, *796*, 123; (c) G. Marin, V. Tudor, V. C. Kravtsov, M. Schmidtmann, Y. A. Simonov, A. Müller and M. Andruh, *Cryst. Growth Des.*, **2005**, *5*, 279; (d) V. Tudor, G. Marin, V. Kravtsov, Y. A. Simonov, J. Lipkowski, M. Brezeanu and M. Andruh, *Inorg. Chim. Acta*, **2003**, *353*, 35; (e) M. Andruh, *Chem. Commun*., **2007**, 2565; (f) M. Andruh, *Pure Appl. Chem.*, **2005**, *77*, 1685.

10. A. W. Addison, T. N. Rao, J. Reedijk, J. van Rijn and G. C. Verschoor, *J. Chem. Soc., Dalton Trans.*, **1984**, 1349.
11. CrysAlis RED, Oxford Diffraction Ltd., Version 1.171.36.32, 2003.
12. O. V. Dolomanov, L. J. Bourhis, R. J. Gildea, J. A. K. Howard and H. Puschmann, *J. Appl. Crystallogr.*, **2009**, *42*, 339.
13. G. M. Sheldrick, *Acta Crystallogr.*, **2008**, *A64*, 112.